ACS APPLIED MATERIALS & INTERFACES

www.acsami.org

Research Article

Nanophase-Separated Copper−Zirconia Composites for Bifunctional Electrochemical CO_2 Conversion to Formic Acid

Anna Strijevskaya, Akira Yamaguchi, Shusaku Shoji, Shigenori Ueda, Ayako Hashimoto, Yu Wen, Aufandra Cakra Wardhana, Ji-Eun Lee, Min Liu, Hideki Abe,* and Masahiro Miyauchi*

Cite This: *ACS Appl. Mater. Interfaces* 2023, 15, 23299−23305

Read Online

ACCESS | Metrics & More | Article Recommendations | Supporting Information

ABSTRACT: A copper−zirconia composite having an evenly distributed lamellar texture, Cu#ZrO_2, was synthesized by promoting nanophase separation of the $Cu_{51}Zr_{14}$ alloy precursor in a mixture of carbon monoxide (CO) and oxygen (O_2). High-resolution electron microscopy revealed that the material consists of interchangeable Cu and t-ZrO_2 phases with an average thickness of 5 nm. Cu#ZrO_2 exhibited enhanced selectivity toward the generation of formic acid (HCOOH) by electrochemical reduction of carbon dioxide (CO_2) in aqueous media at a Faradaic efficiency of 83.5% at −0.9 V versus the reversible hydrogen electrode. In situ Raman spectroscopy has revealed that a bifunctional interplay between the Zr^{4+} sites and the Cu boundary leads to amended reaction selectivity along with a large number of catalytic sites.

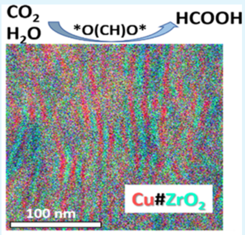

Nanophase-separated catalyst

KEYWORDS: *nanophase separation, $Cu_{51}Zr_{14}$, Cu#ZrO_2, electrochemical CO_2 reduction, bifunctional catalysis, in situ Raman, formic acid*

1. INTRODUCTION

Dependence of humanity on fossil fuels and the resulted emissions of carbon dioxide (CO_2) into the atmosphere created a loop, worsening the world environment. Much effort has been made to reduce the carbon footprint and mitigate the CO_2 emissions as well as to diminish the role of unrenewable fossil fuels in industry. One of the most intensively explored routes is the direct conversion of CO_2 into valuable chemical products including formic acid (FA). The outbreak of COVID-19 results in an increased commercial value of FA due to the high demands in poultry, textile, and pharmaceutical industries.[1] Conventional FA production technologies are based on the hydrolysis of different formates, such as methyl formate, which suffers from poor waste management of toxic byproducts and huge necessity in water supplies.[2] It is desirable to develop highly efficient and selective reaction catalysts that enable the direct conversion of CO_2 to FA without passing through the hydrolysis processes.

Copper (Cu) is an active catalyst for direct CO_2 conversion in terms of its moderate binding ability toward the *CO intermediate and its positive energy for *H adsorption.[3,4] Cu-based catalysts showed a Faradaic efficiency (FE) of 77.1% for direct CO_2 conversion to FA in aqueous media for hollow fibers and 82.4% for carbon-anchored Cu nanoparticles.[5,6] However, such pristine Cu catalysts are poorly selective for FA production, leading to undesired generation of chemical species, including carbon monoxide (CO) and hydrogen (H_2). One of the most promising routes to improve reaction selectivity is the use of metal−oxide interfaces that can promote only the target reaction. Indeed, zirconium oxide (ZrO_2)-supported Cu nanoparticles (ZrO_2/Cu) selectively catalyze the conversion of CO_2 to ethylene (COE).[10] ZrO_2 possesses basic hydroxyl groups (OH) on the surface to efficiently adsorb CO_2 and suppress hydrogen evolution.[7−9] The COE reaction was promoted via a bifunctional mechanism comprising the molecular transfer of a *O(CH)O* intermediate, which was formed on the ZrO_2 surface from adsorbed CO_2, and spilt over to the Cu surface across the Cu−ZrO_2 interface to generate C_{2+} products via an *OCCO* intermediate.[10] The recent study by Li et al. showed that interfacial ZrO_2 favored the stabilization and retention of Cu^+ species in the CuO@ZrO_2 catalyst, which resulted in increased *CO coverage and promoted coupling.[11]

Recently, nanophase separation of alloys has garnered considerable attention as an accessible and scalable path to discover a high density of catalytically active metal−oxide interfaces with a narrow size distribution.[12] Nickel−yttrium oxide (Ni#Y_2O_3) and rhodium−cerium oxide (Rh#CeO_2) were materialized from Ni_2Y and Rh_2Ce precursor alloys, respectively, to demonstrate the enhanced catalytic performances for the dry reforming of methane.[13,14]

Here, we report the use of nanophase separation of a copper−zirconium ($Cu_{51}Zr_{14}$) precursor alloy to obtain a nanocomposite catalyst comprising a metal−metal oxide interface of Cu and ZrO_2 (Cu#ZrO_2). The Cu#ZrO_2 catalyst

Received: February 28, 2023
Accepted: April 21, 2023
Published: May 4, 2023

https://doi.org/10.1021/acsami.3c02874

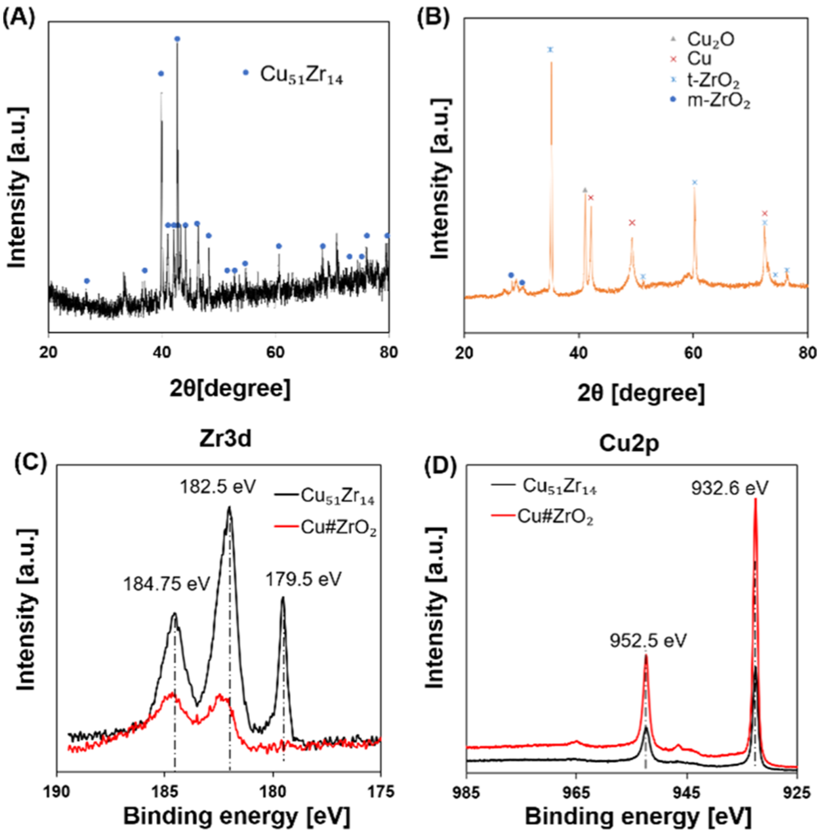

Figure 1. pXRD patterns of the $Cu_{51}Zr_{14}$ precursor alloy (A) and Cu#ZrO_2 (B). HAXPES profiles of the $Cu_{51}Zr_{14}$ precursor alloy (black) and Cu#ZrO_2 (red) in the Zr 3d region (C) and the Cu 2p region (D).

exhibited enhanced selectivity for the electrochemical CO_2 reduction reaction toward FA production in aqueous media through the bifunctional interplay of Cu and ZrO_2 across their interface. Spectroscopic analyses have shown that the CO_2 admolecules on the ZrO_2 surface spill over to the Cu surface across the interface and react with the OH species to generate FA via sequential reaction steps involving $*CO_2^-$ and *OC(H)O*.

2. MATERIALS AND METHODS

2.1. Synthesis of $Cu_{51}Zr_{14}$ Alloy Precursor. An ingot of the $Cu_{51}Zr_{14}$ precursor alloy was obtained by arc-melting of Cu and Zr metals in an argon (Ar) atmosphere. For this process, Cu foil (99.99%, Nilaco Corporation) and Zr chunks (99.99%, Nilaco Corporation) were weighted in a molar ratio of 51:14 placed on a water-cooled copper hearth and subjected to a plasma arc torch. The $Cu_{51}Zr_{14}$ precursor alloy ingot was powdered with an agate mortar in air and sieved to adjust the size of particles to between 40 and 50 μm. The $Cu_{51}Zr_{14}$ powder was placed on a ceramic boat and heated at 400 °C for 12 h in a stream of mixture gases of carbon monoxide (CO)- and oxygen (O_2) at a molar ratio of 2:1 and a total flow rate of 100 mL min^{-1}. The blackish-gray $Cu_{51}Zr_{14}$ powder was converted into a dark-purple nanocomposite of metal Cu and zirconium oxide (ZrO_2), i.e., Cu#ZrO_2.

2.2. Characterization. The synthesized Cu#ZrO_2 material and the $Cu_{51}Zr_{14}$ precursor alloy were characterized by powder X-ray diffraction (pXRD) over a 2θ range of 20−80° with a Rigaku SmartLab diffractometer equipped with a D/teX Ultra detector. The elemental composition and crystallographic structure of the samples were identified with scanning transmission electron microscopy (STEM, JEM-ARM200F, JEOL) imaging equipped with an energy-dispersive X-ray spectrometer (JED-2300, JEOL) operating at an acceleration voltage of 200 kV. A field-emission scanning electron microscope [JSM-7500F (JEOL)] was used to observe the external morphology of the materials. X-ray photoelectron spectroscopy (XPS) was performed after 5 min and 5 h of reaction using an ULVAC-PHI 1600 instrument with a monochromatic Al Kα source. The binding energies were corrected using a carbon (C 1s) signal at 284.80 eV.

Hard X-ray photoemission spectroscopy (HAXPES) measurements were performed at BL15XU of SPring-8 (Super Photon Ring 8 GeV, Hyōgo Prefecture, Japan). The excitation photon energy and total energy resolution were set to 5.95 keV and 240 meV, respectively. The measurements were done at room temperature, and the pressure of the analysis chamber of HAXPES was 1.1 × 10^{-7} Pa.

2.3. Catalyst Preparation. Carbon paper with an average geometrical area of 2 cm^2 was sonicated for 20 min consequently in ethanol and ultrapure water (Millipore Q), after which it was dried in air at 80 °C for 1 h. The catalyst ink was prepared by sonication of 5 mg of Cu#ZrO_2 in a mixture of ethanol (440 μL) and ultrapure water (1785 μL) with an addition of 5 μL of 5% Nafion (Sigma-Aldrich). The prepared ink was then drop-casted onto carbon paper and dried in air at 80 °C for 1 h to ensure evaporation of ethanol. For the purpose of comparison of catalytic activities, we performed the same evaluation protocol on commercial Cu powder (Nilaco Corporation, average particle size: 30 μm), Cu_2O powder (Nilaco Corporation), and a mixture of Cu- and yttria-stabilized zirconia (YSZ, 5.2% Y-doped, Sigma-Aldrich) in a molar ratio 51 to 14. YSZ was chosen as the control due to similarity of phases between ZrO_2 in Cu#ZrO_2 and YSZ. The catalyst loading was always 5 mg for any of the materials.

2.4. Electrochemical CO_2 Reduction. Catalytic activity and selectivity of Cu#ZrO_2 were evaluated in a custom-made H-type cell that was filled with electrolyte solution of 0.1 M $KHCO_3$ (CO_2 saturated, pH 6.8). A silver−silver chloride (Ag/AgCl) electrode and a platinum wire were used as the reference electrode (RE) and counter electrode (CE), respectively. The reaction selectivity was evaluated based on the Faradaic efficiency (FE) that was calculated as follows

$$FE = F \times n \times N/Q \qquad (1)$$

where F, n, N, and Q are the Faradaic constant, number of electrons involved in the reaction, amount of the product in moles, and the total charge that flows between the working and counter electrodes, respectively. Gas product identification was performed using a gas chromatograph equipped with a dielectric-barrier discharge ionization detector (Shimadzu Tracera 2010). A proton nuclear magnetic resonance spectrometer (Bruker UltraShield Plus, 400 MHz) was used for the qualification of liquid products.

2.5. In Situ Spectroscopic Analyses by FT-IR and Raman Spectra. Two sets of measurements were conducted for obtaining diffuse reflectance infrared Fourier transform (DRIFT) spectra. For each of the experiments, a fresh catalyst sample was used, and either nitrogen (N_2) or CO_2 was bubbled through deuterium water (D_2O) for 20−30 min prior to measurements.

In situ Raman spectroscopy was performed using a custom-made steady-flow setup (Figure S1). CO_2-saturated 0.1 M $KHCO_3$ solution is made to flow through a closed chamber with a transparent upper cover from the IN to OUT direction. A working electrode, a RE, and a CE were connected to a flow reactor, and the bias potential was applied from the open-circuit potential (OCP) to −1.0 V vs the reverse hydrogen electrode (RHE). CO_2 gas was continuously bubbled through the electrolyte solution of 0.1 M $KHCO_3$ from 20 min before the experiments onward to keep the setup always saturated with CO_2. The gaseous products of reaction are removed from the chamber with flow of liquid.

3. RESULTS AND DISCUSSION

The pXRD pattern for the alloy precursor (Figure 1A) indicates that the main phase of the precursor was $Cu_{51}Zr_{14}$ ($P6/m$, a = 1.12444 nm, c = 0.82815 nm, $\alpha = \beta = 90°$, $\gamma = 120°$)[15] containing Cu_5Zr ($F\bar{4}3m$, a = 0.68700 nm, $\alpha = \beta = \gamma = 90$).[16] The pXRD pattern for Cu#ZrO_2, shown in Figure 1B, indicates that the prepared Cu#ZrO_2 mainly consisted of metallic Cu (face-centered cubic, $Fm\bar{3}m$; JCPDS no. 85-1326) and tetragonal ZrO_2 (t-ZrO_2, $P4_2/nmc$) with an inclusion of Cu_2O ($Pn\bar{3}m$)[17] and monoclinic ZrO_2 (m-ZrO_2, $P2_1/c$).[18] Note that most of the ZrO_2 phase in Cu#ZrO_2 crystallized in a tetragonal form (t-ZrO_2), which is thermodynamically less favorable than the monoclinic form (m-ZrO_2). Figure 1C,D shows the HAXPES profiles of $Cu_{51}Zr_{14}$ and Cu#ZrO_2. The HAXPES profile of Cu#ZrO_2 in the Zr-3d core region is consistent with the reported data of ZrO_2 (Figure 1C).[19] The Zr^0 $3d_{5/2}$ emission peak positioned at 179.5 eV on the HAXPES profile of $Cu_{51}Zr_{14}$ was not visible on that of Cu#ZrO_2, indicating that the metallic Zr^0 in $Cu_{51}Zr_{14}$ was fully oxidized to ZrO_2 in Cu#ZrO_2.[20,21] Moreover, HAXPES has confirmed that the Cu phase in Cu#ZrO_2 retained the metallic state of Cu^0, the same as in the $Cu_{51}Zr_{14}$ precursor alloy ($2p_{3/2}$: 932.6 eV; $2p_{1/2}$: 952.5 eV) (Figure 1D).

For the investigation of the nanostructure of Cu#ZrO_2, we performed cross-sectional STEM (Figure 2). Elemental mapping images were first acquired with energy-dispersive spectrometry (EDS) for each of the constituent elements such as Cu, Zr, and O. All the STEM−EDS images show a lamellar texture with an average thickness of 5 nm. The Zr- and O species show the same special distributions as part of the ZrO_2 phase in Cu#ZrO_2, where the Cu species are exclusively distributed to the ZrO_2 phase (Figure 2D).

An annular-dark field STEM (ADF-STEM) image of Cu#ZrO_2 near the surface boundary shows that the lamellar structure consists of dark- and bright-contrasted phases (Figure 2E). High-resolution ADF-STEM on the bright-contrasted phase demonstrates a long-range atomic ordering (Figure 2F). A fast Fourier transform (FFT) pattern calculated for the area in the green square box in Figure 2F is assigned to the ⟨010⟩ zone axis of the tetragonal zirconia (t-ZrO_2) (Figure 2F inset), which indicates that the bright-contrasted phase consists of t-ZrO_2. The neighboring, dark-contrasted Cu phase shows an atomic fringe of the Cu(110) plane with a spacing of approximately 0.25 nm.

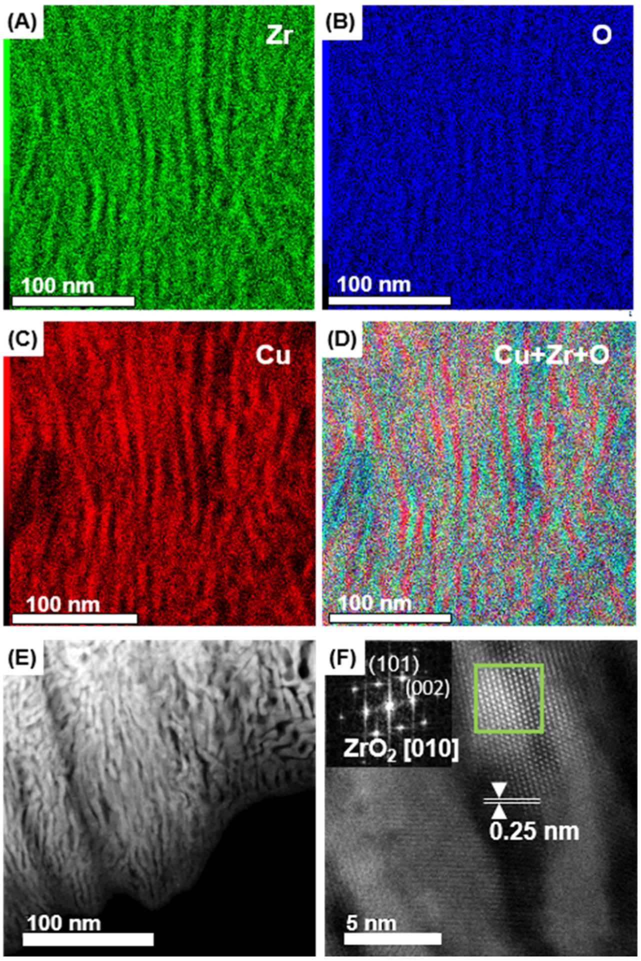

Figure 2. STEM−EDS images of the Cu#ZrO_2 catalyst with a scale bar of 100 nm. Elemental mappings acquired at Zr L (A), O K (B), Cu K (C), and overlapped elemental mapping (D). ADF-STEM image showing a lamellar structure in Cu#ZrO_2 (E). High-resolution ADF-STEM image at the Cu−ZrO_2 boundary and an FFT pattern from the green square area (the inset) (F).

Figure S2 in the Supporting Information shows that Cu#ZrO_2 exhibited larger current densities under CO_2 bubbling than those under an Ar atmosphere (Figure S2A). The changes in current densities in a potential range more anodic than −0.3 V were attributed to a charging caused by the adsorption of CO_2 molecules on the catalyst. Results of cyclic voltammetry shown in Figure S2B indicate the absence of self-oxidation of the catalyst during the electrolysis.

Figure 3A shows the FE of Cu#ZrO_2 for CO_2 reduction at different bias potentials. As indicated by the error bars, the FE values were scattered, but the total FEs were close to 100% under sufficiently negative potentials over −0.4 V vs the RHE. At potentials of more positive than −0.6 V, the major share of FE was occupied by hydrogen evolution. In contrast, at potentials more negative than −0.6 V, FA became one of the most predominant products: the corresponding FEs were 72% (partial current density: 2.4 mA/cm^2) and 83.5% (partial

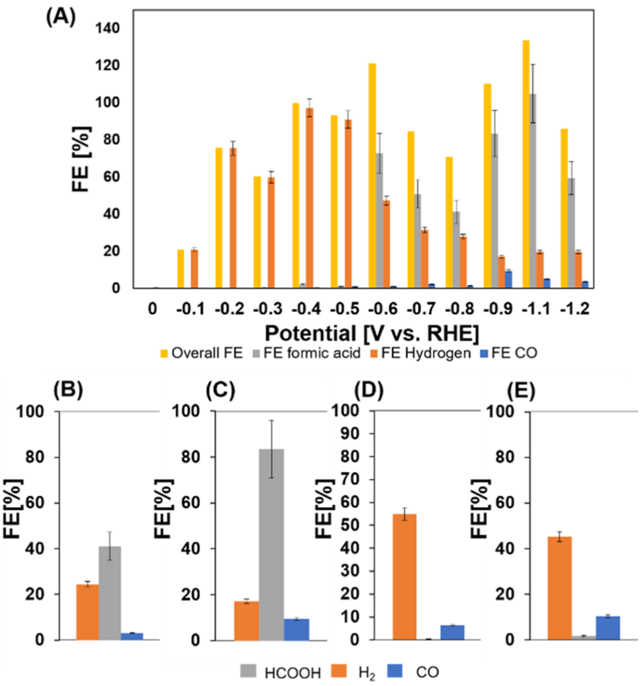

Figure 3. Product distribution of electrochemical CO_2 reduction over Cu#ZrO_2, quantified at the time after 3 h of electrolysis at −0.9 V vs RHE (A).Performance of electrochemical CO_2 reduction over a mixture of Cu + YSZ (B), Cu#ZrO_2 (C), commercial Cu (D), and Cu_2O (E).

current density: 16 mA/cm^2) at −0.6 and −0.9 V, respectively. Hydrogen evolution was only 17% at −0.9 V, which is attributed to the lower hydrogen production selectivity of ZrO_2 as reported by Soloveichik[9] and Li.[11] The other detected products were trace amounts of CH_4 and C_2H_6, constituting less than 1% of FE each as shown in the Supporting Information (Table S1). Based on the result from DFT calculations by Xiao et al.,[22] we can attribute these to enhanced *CO adsorption and dimerization on the Cu^+/Cu^0 pair. We also measured the partial current densities for the FA production (j_{form}) over Cu#ZrO_2 and control catalysts including Cu powder and a powder mixture of Cu- and yttria-stabilized ZrO_2 (Cu + YSZ) (Supporting Information, Figure S3A) since the present ZrO_2 structure in Cu#ZrO_2 is similar to that of YSZ. Among those catalysts, Cu#ZrO_2 exhibited the largest j_{form} at all given potentials. Moreover, Tafel analysis (Figure S3B) showed a slope of 155.9 mV/decade for synthesized Cu#ZrO_2, which is smaller than those of Cu + ZrO_2 and Cu, indicating faster reaction kinetics for CO_2 reduction of our Cu#ZrO_2 catalyst. We also confirmed the absence of reaction products over Cu#ZrO_2 under the argon (Ar) atmosphere, indicating that the products in the CO_2 atmosphere were purely from CO_2 reduction.[23−25] Overall, these results, while being comparable to recent Cu- and Bi-based catalysts, provide valuable insights at interface-related reactions, as shown in the Supporting Information (Table S2).[26,27]

Figure 3B−E shows FEs for FA, H_2, and CO over the different catalysts at the time after 3 h of electrolysis at −0.9 V

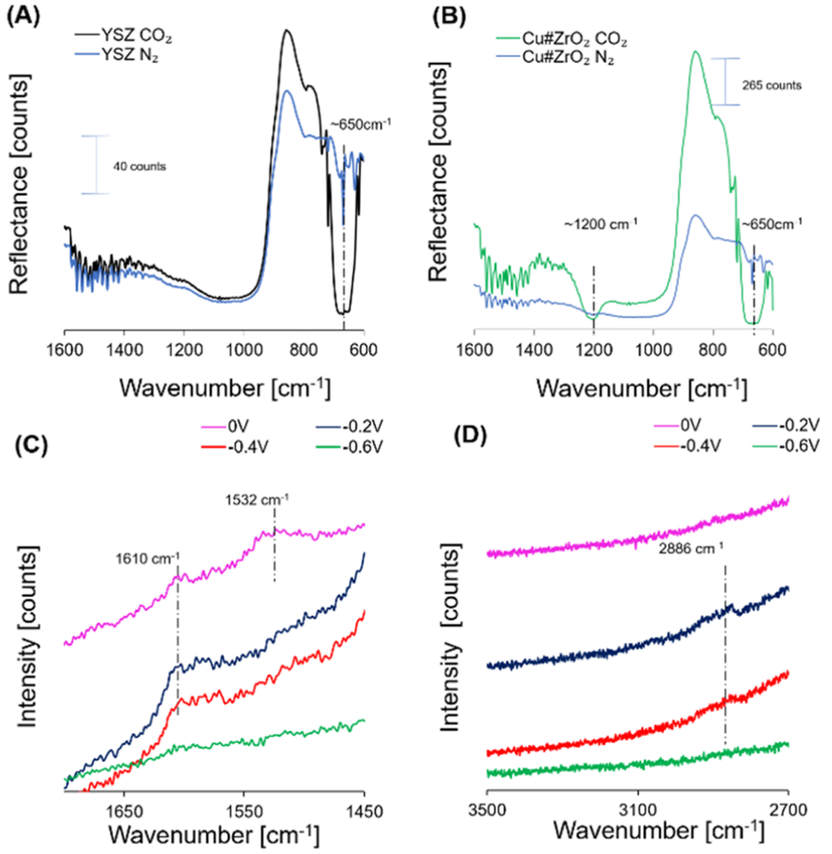

Figure 4. DRIFTS spectra recorded on YSZ (A) and Cu#ZrO_2 (B) under D_2O−CO_2 adsorption. In situ Raman spectra recorded during electrochemical CO_2 reduction at 0.0 V (purple), −0.2 V (blue), −0.4 V (red), and −0.6 V vs RHE (green) over Cu#ZrO_2 in CO_2-saturated 0.1 M $KHCO_3$ (C,D).

vs RHE. The FE for FA generation over the Cu#ZrO_2 and Cu + YSZ catalysts reached 80 and 40%, respectively, whereas neither Cu nor Cu_2O catalysts promoted FA generation. The results showed that the simple mixing of Cu and YSZ is not sufficient to achieve a high FE for FA generation. For the purpose of catalyst characterization after exposure to reaction conditions, FE-SEM and STEM−EDS images were taken after 3 h and 30 min of the electrocatalysis (Figures S4 and S5A−E). Figure S5 indicates the retention of the ZrO_2 phase near the surface of the catalyst grain. Existence of ZrO_2 even after cathodic bias application was further confirmed by XPS (Figure S6) and X-ray fluorescence analyses (Table S3). These results indicate that the catalyst surface is re-constructed at the initial bias application to a Cu-rich nanoporous structure that comprises a stable electrocatalysis center after several hours to stably produce FA. The results of 10 h of the stability test are shown in our Supporting Information (Figure S2C), and we could see the increase of current densities in the initial 4 h of electrocatalytic reaction, which is attributed to the ZrO_2 reduction. After 4 h, the current densities became stable. FE-SEM images, taken before and after the CO_2 reduction reaction, are shown in the Supporting Information (Figure S4).

In order to investigate the role of Cu- and ZrO_2 sites in the molecular adsorption on initial stages of the FA generation reaction, we performed a set of DRIFTS over Cu#ZrO_2 and YSZ in the atmosphere of deuterium oxide (D_2O) vapor and CO_2 (Figure 4A,B). The D_2O vapor atmosphere is useful since it provides a high signal-to-noise ratio in the region of CO_2-related species.[28,29] The results indicate that the broad DRIFTS band around 650 cm^{-1} is attributed to the physisorbed linear CO_2,[30] which is recognized on both the control YSZ and Cu#ZrO_2 under a CO_2 atmosphere (Figure 4A,B). A broad band only observed for Cu#ZrO_2 at around 1200 cm^{-1} (Figure 4B) is likely attributed to the CO_2 molecules chemisorbed to the Cu surface.[31]

Further, we performed in situ Raman spectroscopy on Cu#ZrO_2 using a home-made flowing system filled with a CO_2-saturated aqueous electrolyte of 0.1 M $KHCO_3$ (see the Supporting Information, Figure S1). Figure 4C,D shows the Raman spectra in a potential range from the OCP of 0.0 to −0.6 V vs RHE. A prominent band is recognized at 2886 cm^{-1} over the Cu#ZrO_2 surface in the CO_2 atmosphere at −0.2 V vs RHE (Figure 4D). This band is assigned to the C−H stretching of *O(CH)O*, which strongly correlates with the generation of FA.[32,33] When the potential was more negative than −0.4 V, the peak intensity of *O(CH)O* at 2886 cm^{-1} was decreased, and no other intermediate species were seen in this region. These results suggest that the intermediate species were rapidly converted into FA and desorbed from the catalyst surface under application of high cathodic bias.[34,35] The asymmetric stretching $*CO_2^-$ of adsorbed CO_2 is observed at 1532 cm^{-1}, while 1610 cm^{-1} is assigned to the O−C−O vibration of the adsorbed formate (Figure 4C). Summarizing this spectroscopic data, we propose a possible molecular scenario for the Cu#ZrO_2 catalyst. The CO_2 molecules that were physisorbed on the Zr^{4+} site to result in a reflectance band in DRIFTS 650 cm^{-1} (Figure 4B) were further transferred to the Cu^0 site across the Cu−ZrO_2 interface perimeter for further chemical adsorption (1200 cm^{-1} in DRIFTS, 1532 cm^{-1} in Raman). The protonation of adsorbed CO_2 proceeds through sequential steps involving the formation of *O(CH)O* species (2886 cm^{-1} in Raman) and of the formate species that is identified as a band at 1610 cm^{-1} in Raman.

4. CONCLUSIONS

In conclusion, nanophase-separated Cu#ZrO_2 was successfully obtained by internal oxidation of the $Cu_{51}Zr_{14}$ precursor alloy. Microscopic characterizations have demonstrated that the Cu#ZrO_2 material consists of nanometer-thick lamellae of Cu metal and tetragonal ZrO_2, leading to a stable and widespread Cu−ZrO_2 interface. The Cu#ZrO_2 material exhibits enhanced selectivity toward the electrocatalytic CO_2-to-FA conversion due to the uniformly distributed catalytic sites as well as the abundant metal−oxide interface, which play an important role in amended reaction selectivity. DRIFTS and in situ Raman spectroscopy have shown that CO_2 is adsorbed on the Zr^{4+} site and further protonated into *O(CH)O* over the neighboring Cu site to generate FA via a bifunctional interplay between Cu- and ZrO_2 in Cu#ZrO_2.

■ ASSOCIATED CONTENT

Supporting Information

The Supporting Information is available free of charge at https://pubs.acs.org/doi/10.1021/acsami.3c02874.

Additional experimental data, including experimental setup for in situ Raman measurements (PDF)

■ AUTHOR INFORMATION

Corresponding Authors

Hideki Abe − *National Institute for Materials Science, Tsukuba, Ibaraki 305-0044, Japan; Graduate School of Science and Technology, Saitama University, Saitama 338-8570, Japan;* orcid.org/0000-0002-8392-7586; Email: Abe.Hideki@nims.go.jp

Masahiro Miyauchi − *Department of Materials Science and Engineering, School of Materials and Chemical Technology, Tokyo Institute of Technology, Meguro, Tokyo 152-8552, Japan;* orcid.org/0000-0001-8889-2645; Email: mmiyauchi@ceram.titech.ac.jp

Authors

Anna Strijevskaya − *Department of Materials Science and Engineering, School of Materials and Chemical Technology, Tokyo Institute of Technology, Meguro, Tokyo 152-8552, Japan; Uzbek-Japan Innovation Center of Youth, Tashkent 100095, Uzbekistan*

Akira Yamaguchi − *Department of Materials Science and Engineering, School of Materials and Chemical Technology, Tokyo Institute of Technology, Meguro, Tokyo 152-8552, Japan;* orcid.org/0000-0002-3550-4239

Shusaku Shoji − *Department of Materials Science & Engineering, Cornell University, Ithaca, New York 14853-1501, United States*

Shigenori Ueda − *National Institute for Materials Science, Tsukuba, Ibaraki 305-0044, Japan;* orcid.org/0000-0001-9425-0614

Ayako Hashimoto − *National Institute for Materials Science, Tsukuba, Ibaraki 305-0044, Japan; Graduate School of Pure and Applied Sciences, University of Tsukuba, Tsukuba, Ibaraki 305-8571, Japan*

Yu Wen − *National Institute for Materials Science, Tsukuba, Ibaraki 305-0044, Japan; Graduate School of Pure and*

Applied Sciences, University of Tsukuba, Tsukuba, Ibaraki 305-8571, Japan

Aufandra Cakra Wardhana − *Department of Materials Science and Engineering, School of Materials and Chemical Technology, Tokyo Institute of Technology, Meguro, Tokyo 152-8552, Japan*

Ji-Eun Lee − *Biofunctional Catalyst Research Team, RIKEN Center for Sustainable Resource Science, Wako, Saitama 351-0198, Japan*

Min Liu − *Hunan Joint International Research Center for Carbon Dioxide Resource Utilization, School of Physical and Electronics, Central South University, Changsha 410083, Public Republic of China;* orcid.org/0000-0002-9007-4817

Complete contact information is available at:
https://pubs.acs.org/10.1021/acsami.3c02874

Author Contributions

A.S. dealt with the experimental investigation, data analysis, and first draft writing; A.Y. took care of the supervision and electrochemical analysis; S.S. took charge of the conceptualization; A.H. and Y.W. performed the electron microscope analysis; A.C.W. did the XPS measurements and analysis; J.-E.L. took charge of the in situ Raman spectroscopy analysis; S.U. performed the HAXPES measurement and analysis; M.L. was in charge of the supervision; H.A. took charge of the establishment of the synthetic method of the nanophase-separated structure, supervision, and writing the manuscript; M.M. conducted the supervision, funding, and writing the final manuscript and was the project leader.

Notes

The authors declare no competing financial interest.

■ ACKNOWLEDGMENTS

This work was funded by JST SICORP (no. JPMJSC18H7) and the Japan International Cooperation Agency (JICA)-Knowledge Co-creation Program and was also supported by the JST CREST program (grant no. JPMJCR15P1) toward "Innovative Catalysts". We also thank the Human Joint International Research Center for Carbon Dioxide Resource Utilization, School of Physical and Electronics, Central South University, Changsha, Republic of China. The TEM characterization was carried out using the NIMS TEM Station facility and supported by the Global Research Center for Environment and Energy. HAXPES measurements were performed with approval from the NIMS Synchrotron X-ray Station (proposal nos. 2, 019A4600, 2019B4600, 2020A4600, 2020A4605). The authors thank Dr. Kadirova Z. Ch. for the program initiation.

■ REFERENCES

(1) Rieser, K.-P. *BASF Increases Prices for Formic Acid and for Propionic Acid*; The BASF News Release, 2020; Vol. *20*, p 364.

(2) Hietala, J.; Vuori, A.; Johnsson, P.; Pollari, I.; Reutemann, W.; Kieczka, H. Formic Acid. *Ullmann's Encycl. Ind. Chem.* **2016**, *A12*, 1−22.

(3) Hori, Y. Electrochemical CO_2 Reduction on Metal Electrodes. In *Modern Aspects of Electrochemistry In Modern Aspects of Electrochemistry*; Vayenas, C. G., White, R. E., Gamboa-Aldeco, M. E., Eds.; Springer: New York, 2008; Vol. *42*, pp 89−189.

(4) Bagger, A.; Ju, W.; Varela, A. S.; Strasser, P.; Rossmeisl, J. Electrochemical CO_2 Reduction: A Classification Problem. *ChemPhysChem* **2017**, *18*, 3266−3273.

(5) Liu, D.; Hu, Y.; Shoko, E.; Yu, H.; Isimjan, T. T.; Yang, X. High Selectivity of CO_2 Conversion to Formate by Porous Copper Hollow Fiber: Microstructure and Pressure Effects. *Electrochim. Acta* **2021**, *365*, 137343.

(6) Du, J.; Xin, Y.; Dong, M.; Yang, J.; Xu, Q.; Liu, H.; Han, B. Copper/Carbon Heterogenous Interfaces for Enhanced Selective Electrocatalytic Reduction of CO_2 to Formate. *Small* **2021**, *17*, 2102629.

(7) Cheng, F.; Tompsett, G. A.; Fraga Alvarez, D. V.; Romo, C. I.; McKenna, A. M. S.; Niles, F.; Nelson, R. K.; Reddy, C. M.; Granados-Focil, S.; Paulsen, A. D.; Zhang, R.; Timko, M. T. Metal Oxide Supported Ni-Impregnated Bifunctional Catalysts for Controlling Char Formation and Maximizing Energy Recovery During Catalytic Hydrothermal Lliquefaction of Food Waste. *Sustainable Energy Fuels* **2021**, *5*, 941−955.

(8) Wang, H.; Lee, H. W.; Deng, Y.; Lu, Z.; Hsu, P. C.; Liu, Y.; Lin, D.; Cui, Y. Bifunctional Non-noble Metal Oxide Nanoparticle Electrocatalysts Through Lithium-induced Conversion for Overall Water Splitting. *Nat. Commun.* **2015**, *6*, 7261−7268.

(9) Soloveichik, G. Electrochemical Synthesis of Ammonia as a Potential Alternative to the Haber−Bosch Process. *Nat. Catal.* **2019**, *2*, 377−380.

(10) Guo, P.; He, Z.; Yang, S.; Wang, W.; Wang, K.; Li, C.; Wei, Y.; Liu, Z.; Han, B. Electrocatalytic CO_2 Reduction to Ethylene over ZrO_2/Cu-Cu_2O Catalysts in Aqueous Electrolytes. *Green Chem.* **2022**, *24*, 1527−1533.

(11) Li, X.; Li, L.; Xia, Q.; Hong, S.; Hao, L.; Robertson, A. W.; Zhang, H.; Benedict Lo, T. W.; Sun, Z. Selective Electroreduction of CO_2 and CO to C_2H_4 by Synergistically Tuning Nanocavities and the Surface Charge of Copper Oxide. *ACS Sustainable Chem. Eng.* **2022**, *10*, 6466−6475.

(12) Najib, A. S. B. M.; Peng, X.; Hashimoto, A.; Shoji, S.; Iida, T.; Bai, Y.; Abe, H. Mesoporous Rh Emerging from Nanophase-separated Rh-Y Alloy. *Chem.−Asian J.* **2019**, *14*, 2802−2805.

(13) Tanabe, T.; Imai, T.; Tokunaga, T.; Arai, S.; Yamamoto, Y.; Ueda, S.; Ramesh, G. V.; Nagao, S.; Hirata, H.; Matsumoto, S.; Fujita, T.; Abe, H. Nanophase-separated Ni_3Nb as an Automobile Exhaust Catalyst. *Chem. Sci.* **2017**, *8*, 3374−3378.

(14) Shoji, S.; Peng, X.; Imai, T.; Murphin Kumar, P. S.; Higuchi, K.; Yamamoto, Y.; Tokunaga, T.; Arai, S.; Ueda, S.; Hashimoto, A.; Tsubaki, N.; Miyauchi, M.; Fujita, T.; Abe, H. TopologicallyImmobilized Catalysis Centre for Long-term Stable Carbon Dioxide Reforming of Methane. *Chem. Sci.* **2019**, *10*, 3701−3705.

(15) Gabathuler, J. P.; White, P.; Parthé, E. $Zr_{14}Cu_{51}$ and $Hf_{14}Cu_{51}$ with $GdAg_3$. 6 Structure Type. *Acta Crystallogr., Sect. B: Struct. Sci., Cryst. Eng. Mater.* **1975**, *31*, 608−610.

(16) Forey, P.; Glimois, J. L.; Feron, J. L. Etudes Structurales et Physiques D'alliages Riches en Cuivre dans le Systeme Cu-Zr. *J. Less-Common Met.* **1986**, *124*, 21−27.

(17) Neuburger, M. C. Präzisionsmessung der Gitterkonstante von Cuprooxyd Cu2O. *Z. Physik* **1931**, *67*, 845−850.

(18) Bouvier, P.; Djurado, E.; Ritter, C.; Dianoux, A.; Lucazeau, G. Low Temperature Phase Transformation of Nanocrystalline Tetragonal ZrO2 by Neutron and Raman Scattering Studies. *Solid State Sci.* **2001**, *3*, 647−654.

(19) Liu, J.; Liao, M.; Imura, M.; Tanaka, A.; Iwai, H.; Koide, Y. Low On-resistance Diamond Field Effect Transistor with High-k ZrO_2 as Dielectric. *Sci. Rep.* **2014**, *4*, 6395.

(20) Li, Y.; Zhao, G.; Zhu, R.; Kou, Z. X ray Photoelectron Spectroscopy (XPS) Analysis of Photosensitive ZrO_2 Array. In *IOP Conference Series: Materials Science and Engineering*; IOP Publishing, 2018; Vol. *322*, p 022043.

(21) Lackner, P.; Zou, Z.; Mayr, S.; Diebold, U.; Schmid, M. Using photoelectron spectroscopy to observe oxygen spillover to zirconia. *Phys. Chem. Chem. Phys.* **2019**, *21*, 17613−17620.

(22) Xiao, H.; Goddard, W. A., III; Cheng, T.; Liu, Y. Cu Metal Embedded in Oxidized Matrix Catalyst to Promote CO_2 Activation and CO Dimerization for Electrochemical Reduction of CO_2. *PNAS* **2017**, *114*, 6685−6688.

(23) Bonet, N. A.; Nogalska, A.; Garcia-Valls, R. Direct Electrochemical Reduction of Bicarbonate to Formate Using Tin Catalyst. *Electrochem* **2021**, *2*, 64−70.

(24) Zhong, H.; Fujii, K.; Nakano, Y. Effect of $KHCO_3$ Concentration on Electrochemical Reduction of CO_2 on Copper Electrode. *J. Electrochem. Soc.* **2017**, *164*, F923−F927.

(25) Xiang, H.; Miller, H. A.; Bellini, M.; Christensen, H.; Scott, K.; Rasul, S.; Yu, E. H. Production of Formate by CO_2 Electrochemical Reduction and its Application in Energy Storage. *Sustain* **2020**, *4*, 277−284.

(26) Li, D.; Liu, T.; Huang, L.; Wu, J.; Li, J.; Zhen, L.; Feng, Y. Selective CO_2-to-Formate Electrochemical Conversion with Core−Shell Structured Cu_2O/Cu@C Composites Immobilized on Nitrogen-Doped Graphene Sheets. *J. Mater. Chem. A.* **2020**, *8*, 18302−18309.

(27) Tao, Z.; Wu, Z.; Wu, Y.; Wang, H. Activating Copper for Electrocatalytic CO_2 Reduction to Formate via Molecular Interactions. *ACS Catal.* **2020**, *10*, 9271−9275.

(28) Nakamoto, K. *Infrared and Raman Spectra of Inorganic and Coordination Compounds*; John Wiely & Sons, Ins., 6th edn, 2008; Chapter 1, p 1.

(29) Nakamoto, K. *Infrared and Raman Spectra of Inorganic and Coordination Compounds*; John Wiely & Sons, Ins., 6th edn, 2008; Chapter 2, p 275.

(30) Taifan, W.; Boily, J. F.; Baltrusaitis, J. Surface Chemistry of Carbon Dioxide Revisited. *Surf. Sci. Rep.* **2016**, *71*, 595−671.

(31) Bersani, M.; Gupta, K.; Mishra, A. K.; Lanza, R.; Taylor, S. F. R.; Islam, H. U.; Hollingsworth, N.; Hardacre, C.; de Leeuw, N. H.; Darr, J. A. Combined EXAFS, XRD, DRIFTS, and DFT Study of Nano Copper-based Catalysts for CO_2 Hydrogenation. *ACS Catal.* **2016**, *6*, 5823−5833.

(32) Chernyshova, I. V.; Somasundaran, P.; Ponnurangam, S. On the Origin of the Elusive First Intermediate of CO_2 Electroreduction. *PNAS* **2018**, *115*, E9261−E9270.

(33) Jiang, S.; Klingan, K.; Pasquini, C.; Dau, H. New Aspects of Operando Raman Spectroscopy Applied to Electrochemical CO_2 Reduction on Cu Foams. *J. Chem. Phys.* **2019**, *150*, 041718.

(34) Yoo, J. S.; Christensen, R.; Vegge, T.; Nørskov, J. K.; Studt, F. Theoretical Iinsight into the Trends that Guide the Electrochemical Reduction of Carbon Dioxide to Formic Acid. *ChemSusChem* **2016**, *9*, 358−363.

(35) Tao, Z.; Wu, Z.; Wu, Y.; Wang, H. Activating Copper for Electrocatalytic CO_2 Reduction to Formate via Molecular Interactions. *ACS Catal.* **2020**, *10*, 9271−9275.